STRUCTURAL CHEMISTRY

Volume 76 (2020)

Supporting information for article:

Tracking the dissolution–recrystallization structural transformation (DRST) of copper(II) complexes: a combined crystallographic, mass spectrometric and DFT study

Qian-Jun Deng, Min Chen, Dong-Chu Chen, Hang-Yu Long and Chang-Ai Chen

Supporting Tables	
Table S1	DRST literature summary.
Table S2	(a) Crystallographic data of the complexes **Cu1** and **Cu2**; (b) Selected bond lengths (Å) and angles (°) of **Cu1** and **Cu2**.
Table S3~S4	*SHAPE* analysis of the Cu1 ion in **Cu1** and Cu1 ions in **Cu2**.
Table S5	Hirshfeld surfaces mapped with d_{norm} (left) showing Shape-index (middle) and Curvedness (right) for the **Cu1** and **Cu2**.
Table S6	Fingerprint plot for different interactions for **Cu1** and **Cu2** showing the percentage of contacts created to the total Hirshfeld surface area of the **Cu1** and **Cu2** molecules.
Table S7	Bond order analysis of **Cu1**. Atomic labels are shown below the table.
Table S8	Calculated orbitals energy for ESI-MS fragments using B3LYP functional and SDD (for Fe)/6-311G* (for other elements) with Gaussian 16 software.
Supporting Figures	
Scheme S1	(a) Introduction to the concept of structural transformation (ST). (b) SciFinder queries the number of related documents obtained after screening the above keywords, and the deadline is October 20, 2019.
Figure S1a	Major species assigned in the ESI-MS of **Cu1** in positive mode
Figure S1b	**Cu1** (a) and **Cu2** (b) intermolecular stacking diagrams.
Figure S2	Thermogravimetry of the compounds at a heating rate of 5 °C/min under N_2 atmosphere for **Cu1** and **Cu2**.
Figure S3	Powdered X-ray diffraction (PXRD) patterns for **Cu1** and **Cu2**.
Figure S4	ESI-MS test results of **Cu1** single crystals at different ion source voltages.
Figure S5	ESI-MS anion model test of **Cu1** at different ion source voltages.
Figure S6	ESI-MS test cation model fitting of **Cu1** single crystals at different ion source voltages.
Figure S7	ESI-MS traces the conversion of **Cu1** to **Cu2** in methanol at 60 °C.
Figure S8	Major species assigned in the ESI-MS of **Cu1** in positive mode.

Figure S9	Cell cycle of HeLa tumor cells after treatment with Cu(II) complexes **2** (3 μM, 6 μM, 9 μM) for 24 h compared with untreated cells.

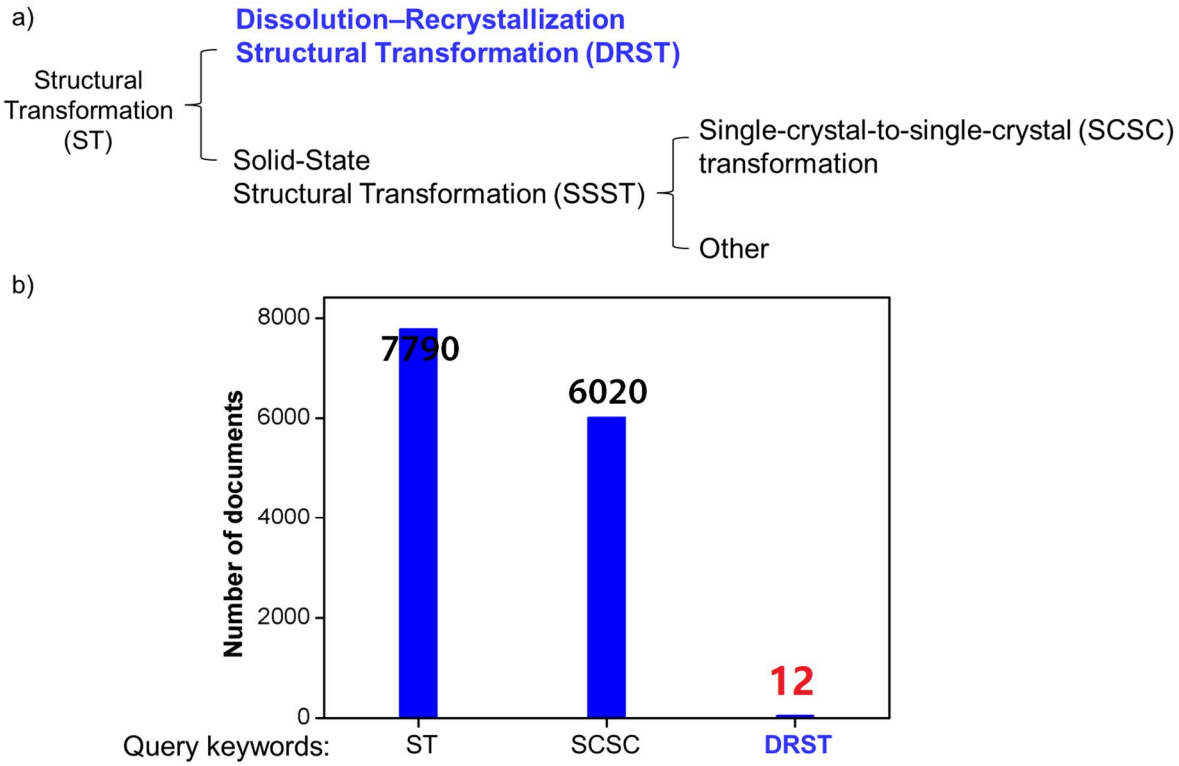

Scheme S1. (a) Introduction to the concept of structural transformation (ST); (b) SciFinder queries the number of related documents obtained after screening the above keywords, and the deadline is October 20, 2019.

Table S1. DRST literature summary.

No.	Title	Research method	Ref.	DRST mechanism research
1	Single-crystal-to-single-crystal (SCSC) transformation and dissolution–recrystallization structural transformation (DRST) among three new copper(II) coordination polymers	Crystallographic	*CrystEngComm.* **2018**, *20*, 570–577.	No

2	Diverse dissolution–recrystallization structural transformations and sequential Förster resonance energy transfer behavior of a luminescent porous Cd-MOF	Crystallographic	*Dalton Trans.* **2017**, *46*, 11656-11663.	No
3	The effect of solvent on one-dimensional cadmium coordination polymers	Crystallographic	*New J. Chem.* **2018**, *42*, 15014-15021.	*No*
4	Unveiling the Mechanism of Water-Triggered Diplex Transformation and Correlating the Changes in Structures and Separation Properties	Crystallographic	*Adv. Funct. Mater.* **2015**, *25*, 6448–6457.	*No*
5	Assessing the Risk of Salt Disproportionation Using Crystal Structure and Surface Topography Analysis	Crystallographic	**DOI:** 10.1021/acs.cgd.8b01188	*No*
6	Irreversible Solvent-Assisted Structural Transformation in 3D Metal-organic Frameworks: Structural Modification and Enhanced Iodine-Adsorption Properties	Crystallographic	*Spectrochim. Acta Part A Mol. Biomol. Spectrosc.* **2018**, *205*, 139–145.	*No*
7	Enhancement of CO_2 adsorption and separation for non-porous Zn/Co azolate frameworks via ethanol-induced structural transformation	Crystallographic	**DOI:** 10.1016/j.jtice.2018.04.025	*No*
8	Same not the Same: Thermally-Driven Transformation of Nickel	Crystallographic	*Cryst. Growth Des.* **2018**, *18*, 2234–2242.	*No*

	Phosphinate-Bipyridine 1D Chains into 3D Coordination Polymers			
9	Hydrothermal syntheses and anion-induced structural transformation of three Cadmium phosphonates	Crystallographic	**DOI:** 10.1016/j.jssc.2018.02.005	*No*
10	Hierarchical MFI zeolite synthesized via regulating the kinetic of dissolution-recrystallization and their catalytic properties	Crystallographic	*Catal. Commun.* **2018**, *115*, 82–86.	*No*
11	Mechanisms of Solvent-Mediated Structural Transformations for Dynamic Crystals of Coordination Supramolecular Systems	Crystallographic	*Chem. Eur. J.* **2018**, *24,* 13072-13077.	*No*
12	Structural Transformations of Pb(II)-trans-1,2-bis(4′-pyridyl)ethene Coordination Polymers in Solution	Crystallographic	*Cryst. Growth Des.* **2011**, *11*, 4697–4703.	*No*
13	Tracking the Dissolution-Recrystallization Structural Transformation (DRST) of Copper(II) Complexes: A Combined Crystallographic, Mass Spectrometric and DFT Study	Crystallographic, ESI-MS and DFT	***This work***	***Yes***

Table S2a. Crystallographic data of the complexes **Cu1** and **Cu2**.

Complex	**Cu1**	**Cu2**
Formula	$C_{22}H_{18}CuN_4O_2S_2$	$C_{24}H_{24}Cu_2N_4O_4S_2$
Formula weight	498.06	623.67
T (K)	293(2)	293(2)
Crystal system	Trigonal	Triclinic
Space group	$P3_221$	*P*-1

a (Å)	9.7940(3)	7.5050(11)
b (Å)	9.7940(3)	7.9967(7)
c (Å)	19.8673(8)	11.9102(19)
α (°)	90.00	76.112(10)
β (°)	90.00	71.827(14)
γ (°)	120.00	82.057(9)
V (Å^3)	1650.40(10)	657.73(15)
Z	3	1
D_c (g cm^{-3})	1.503	1.575
μ (mm^{-1})	1.209	1.813
F(000)	765.0	318.0
Reflns coll.	8097	7895
Unique reflns	2159	2296
R_{int}	0.0368	0.0959
[a]R_1 [$I \geq 2\sigma(I)$]	0.0561	0.0814
[b]wR_2 (all data)	0.1539	0.2340
GOF	1.104	1.152

[a]$R_1 = \Sigma||F_o|-|F_c||/\Sigma|F_o|$, [b]$wR_2 = [\Sigma w(F_o^2-F_c^2)^2/\Sigma w(F_o^2)^2]^{1/2}$

Table S2b. Selected bond lengths (Å) and angles (°) of **Cu1** and **Cu2**.

Cu1					
Cu1—O1	2.432 (4)	Cu1—N1^i	2.034 (4)	Cu1—N2	1.932 (6)
Cu1—O1^i	2.432 (4)	Cu1—N1	2.034 (4)	Cu1—N2^i	1.932 (6)
O1^i—Cu1—O1	166.6 (2)	N1^i—Cu1—N1	90.8 (2)	N2—Cu1—N1	89.8 (2)
N1—Cu1—O1	73.10 (15)	N2—Cu1—O1^i	93.7 (2)	N2—Cu1—N1^i	166.8 (2)
N1^i—Cu1—O1^i	73.10 (15)	N2—Cu1—O1	95.5 (2)	N2^i—Cu1—N1^i	89.8 (2)
N1—Cu1—O1^i	97.27 (15)	N2^i—Cu1—O1^i	95.5 (2)	N2^i—Cu1—N1	166.8 (2)

N1^{i}—Cu1—O1	97.27 (15)	N2^{i}—Cu1—O1	93.7 (2)	N2^{i}—Cu1—N2	92.5 (4)
Symmetry code: (i) -*x*, -*x*+*y*, -*z*+2/3.					
Cu2					
Cu1—Cu1^{i}	3.008 (2)	Cu1—O1^{i}	1.920 (5)	Cu1—N2	1.992 (6)
Cu1—O1	1.923 (6)	Cu1—O2	2.379 (5)	Cu1—N1	1.949 (7)
O1^{i}—Cu1—O1	77.0 (2)	O1^{i}—Cu1—N2	170.6 (2)	N2—Cu1—O2	73.3 (2)
O1—Cu1—O2	95.3 (2)	O1—Cu1—N2	95.4 (2)	N1—Cu1—O2	102.0 (3)
O1^{i}—Cu1—O2	101.7 (2)	O1—Cu1—N1	162.5 (3)	N1—Cu1—N2	92.3 (3)
O1^{i}—Cu1—N1	96.5 (3)	Cu1^{i}—O1—Cu1	103.0 (2)		
Symmetry code: (i) -*x*+1, -*y*+1, -*z*+2.					

Table S3. *SHAPE* analysis of the Cu1 ion in **Cu1**.

Label	Shape	Symmetry	Distortion (º)
HP-6	D_{6h}	Hexagon	30.467
PPY-6	C_{5v}	Quadrangular pyramid	24.497
OC-6	O_h	Octahedron	2.387
TPR-6	D_{3h}	Trigonal prism	13.896
JPPY-6	C_{5v}	Johnson quadrangular pyramid J2	27.648

Table S4. *SHAPE* analysis of the Cu1 ion in **Cu2**.

Label	Shape	Symmetry	Distortion (º)
PP-5	D_{5h}	Hexagon	26.719
vOC-5	C_{4v}	Quadrangular pyramid	2.967
TBPY-5	D_{3h}	Octahedron	4.383

SPY-5	C_{4v}	Trigonal prism	2.701
JTBPY-5	D_{3h}	Johnson quadrangular pyramid J2	7.521

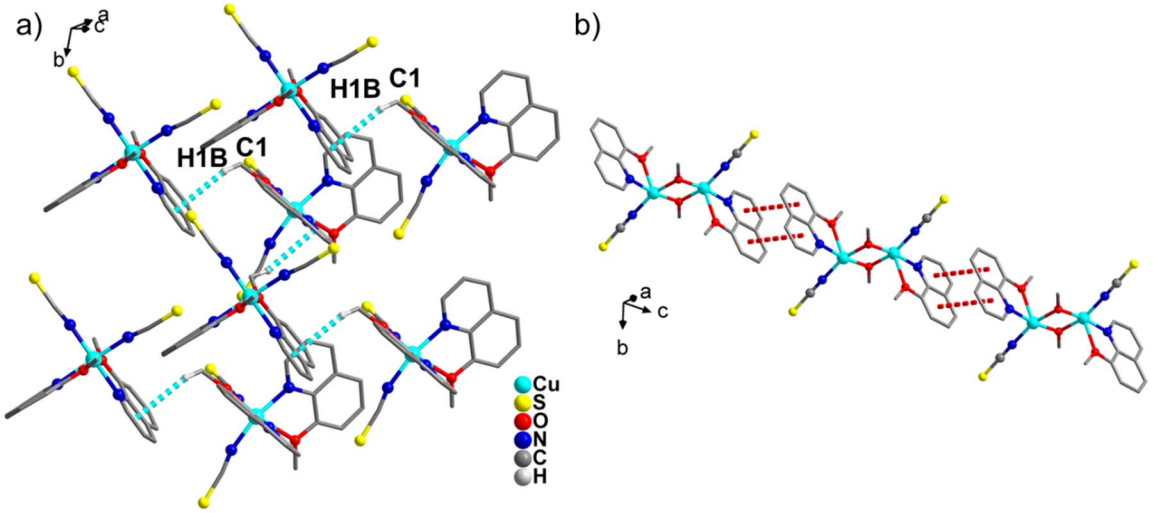

Figure S1a. The intermolecular weak interaction between **Cu1** (a) and **Cu2** (b).

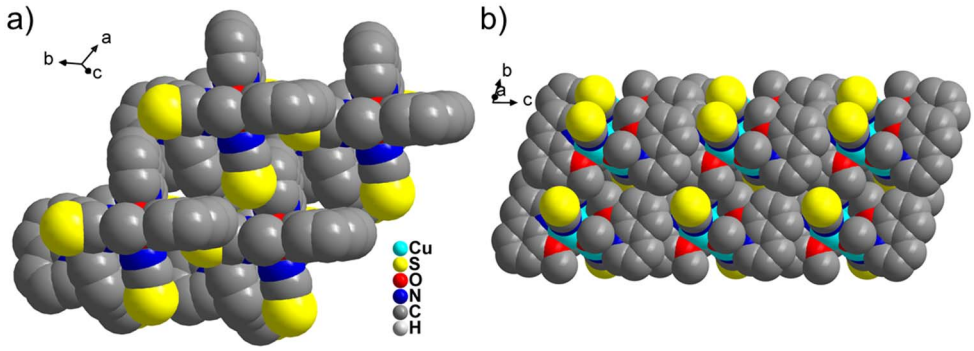

Figure S1b. Cu1 (a) and **Cu2** (b) intermolecular stacking diagrams.

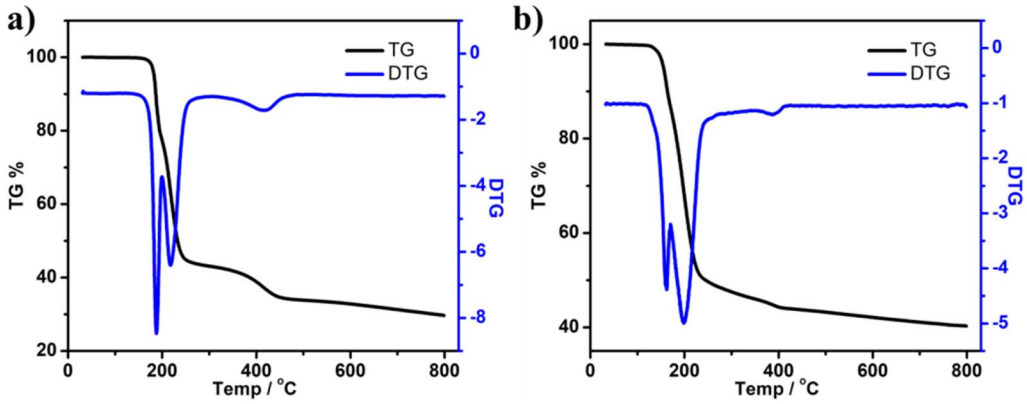

Figure S2. Thermogravimetry of the compounds at a heating rate of 5 °C/min under N_2 atmosphere for **Cu1** (a) and **Cu2** (b).

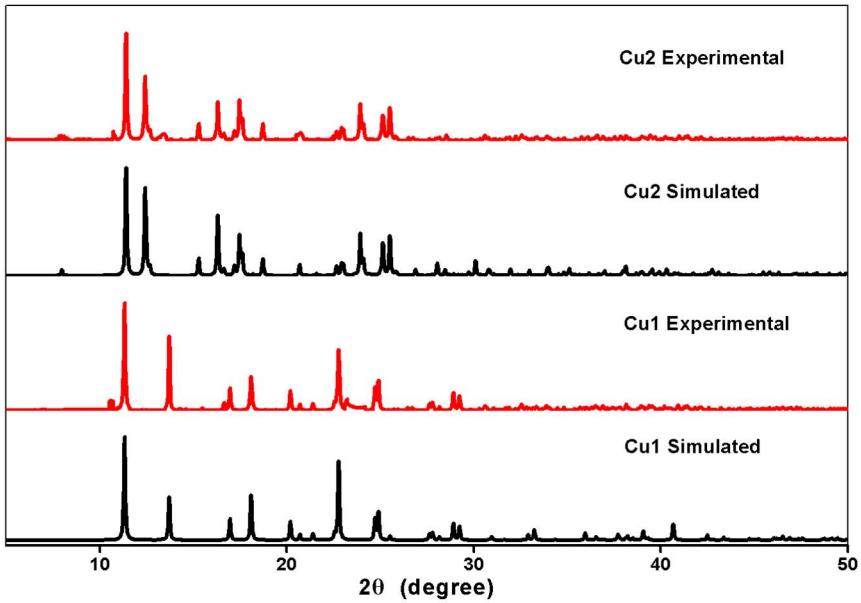

Figure S3. Powdered X-ray diffraction (PXRD) patterns for **Cu1** and **Cu2**.

Table S5. Hirshfeld surfaces mapped with d_{norm} (left) showing Shape-index (middle) and Curvedness (right) for the **Cu1** and **Cu2**. Hirshfeld surface analysis were performed using CrystalExplorer (Version 3.1), S. K. Wolff, D. J. Grimwood, J. J. McKinnon, M. J. Turner, D. Jayatilaka, M. A. Spackman, University of Western Australia, 2012.

	d_{norm}	Shape Index	Curvedness
Cu1	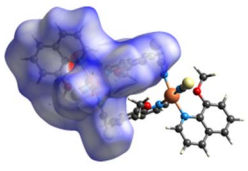	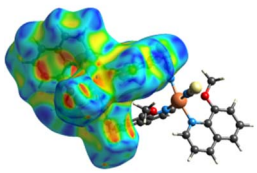	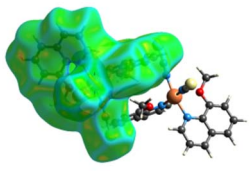
	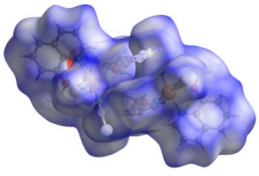	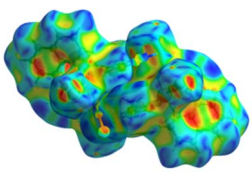	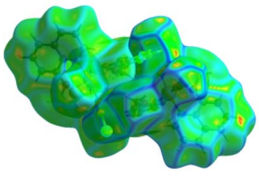

Cu2	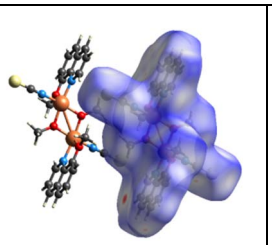	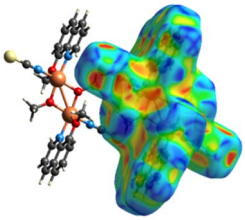	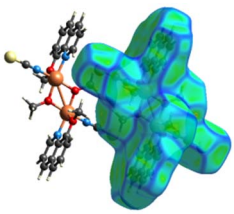
	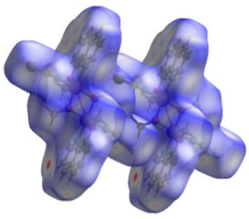	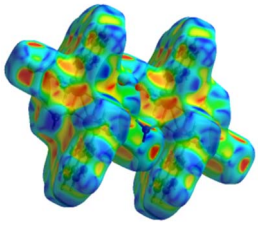	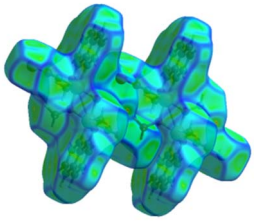

Table S6. Fingerprint plot for different interactions for **Cu1** and **Cu2** showing the percentage of contacts created to the total Hirshfeld surface area of the **Cu1** and **Cu2** molecules. d_i is the closest internal distance from a given point on the Hirshfeld surface; d_e is the closest external contact.

Inside + outside	Cu1	Cu2
All···All	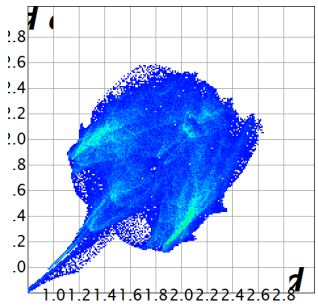	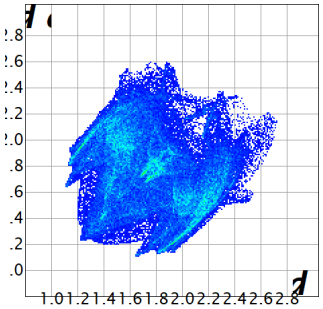
All···H	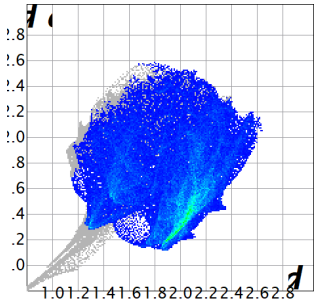	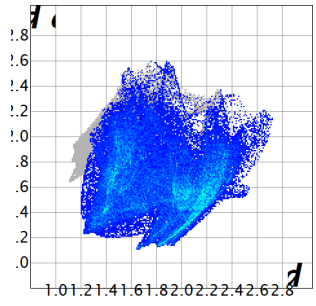
H···H	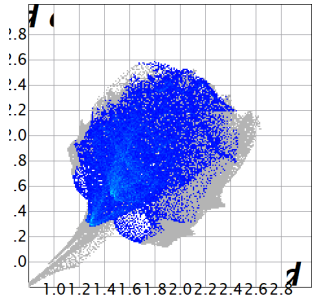	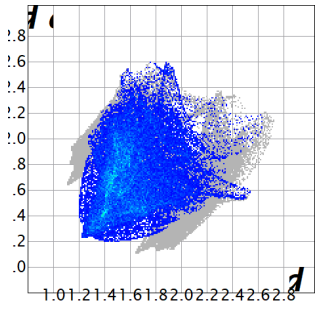

S···H	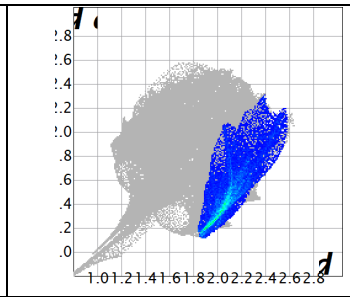	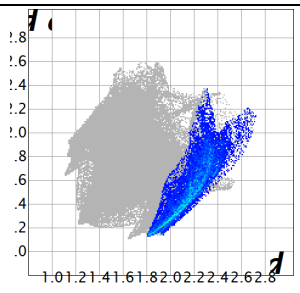
O···H	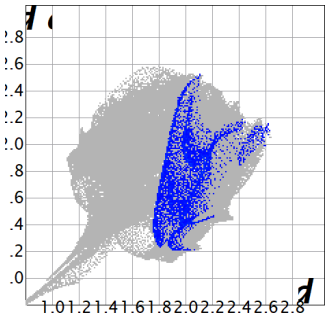	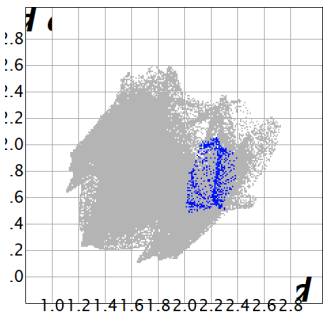

Table S7. Bond order analysis of **Cu1**. Atomic labels are shown below the table.

	Bond length (Å)	Wiberg bond order analysis in Lowdin orthogonalized basis	Fuzzy bond order analysis	Mulliken bond ordre analysis
Cu1-N8	1.933	0.76791525	1.05039582	-3.16500075
Cu1-N32	1.933	0.76785547	1.05030593	-3.16306383
Cu1-N28	2.034	0.52898128	0.82011796	-2.84006094
Cu1-N4	2.033	0.52899460	0.82012879	-2.84020043
Cu1-O3	2.433	0.24233775	0.44062508	-0.92722961
Cu1-O27	2.432	0.24233301	0.44061725	-0.92724642

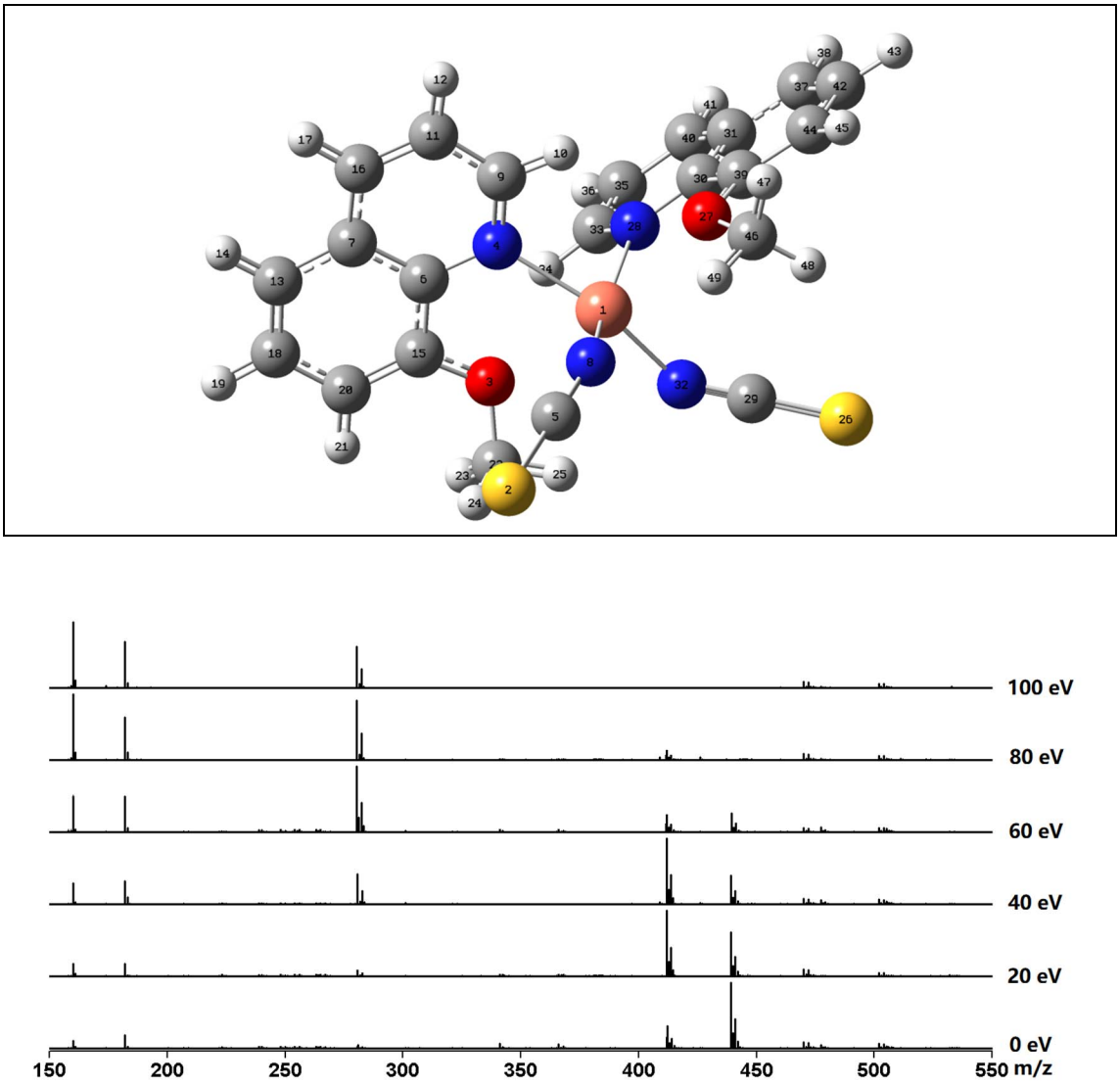

Figure S4. ESI-MS test results of **Cu1** single crystals at different ion source voltages.

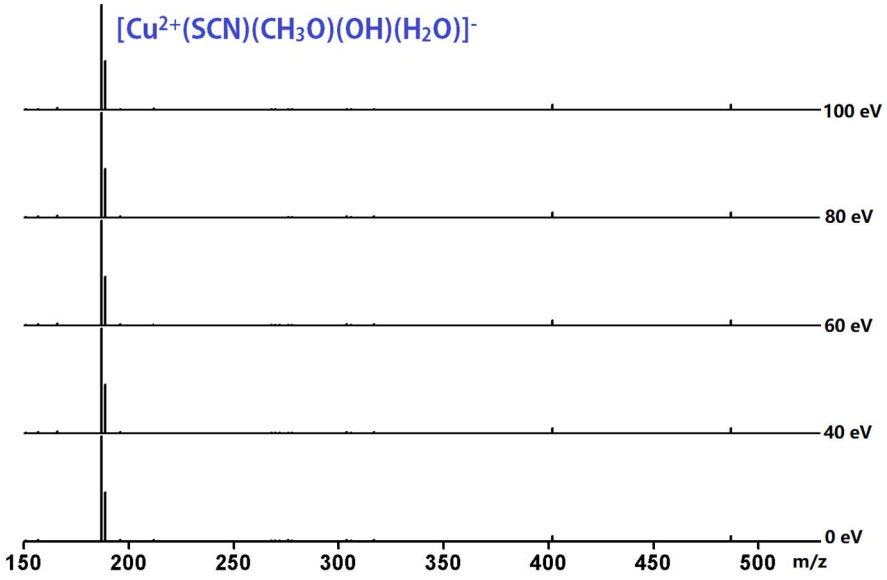

Figure S5. ESI-MS anion model test of **Cu1** at different ion source voltages.

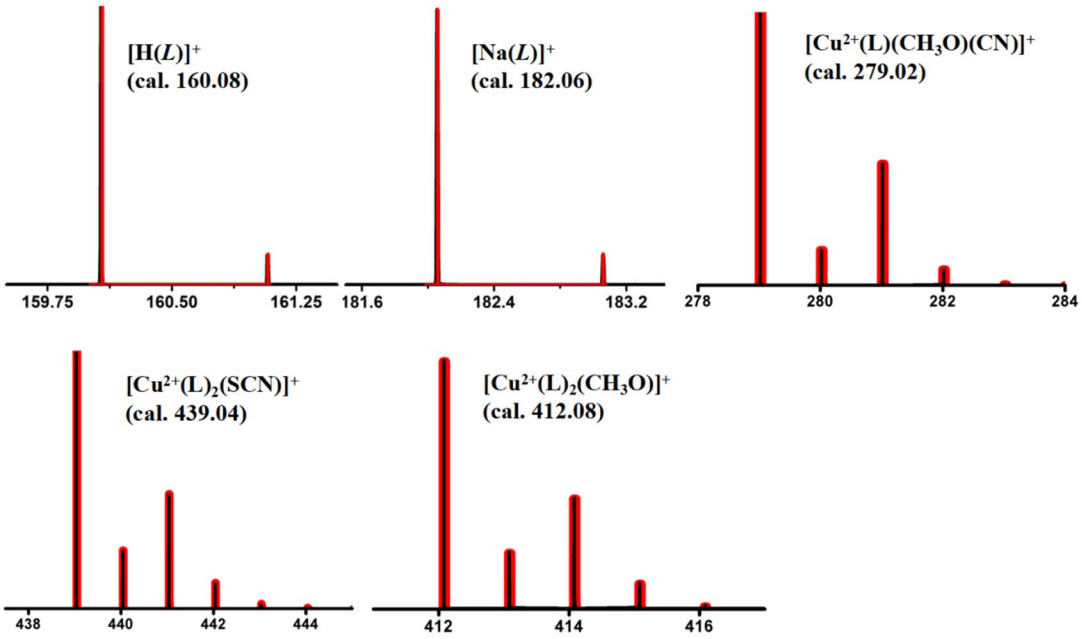

Figure S6. ESI-MS test cation model fitting of **Cu1** single crystals at different ion source voltages.

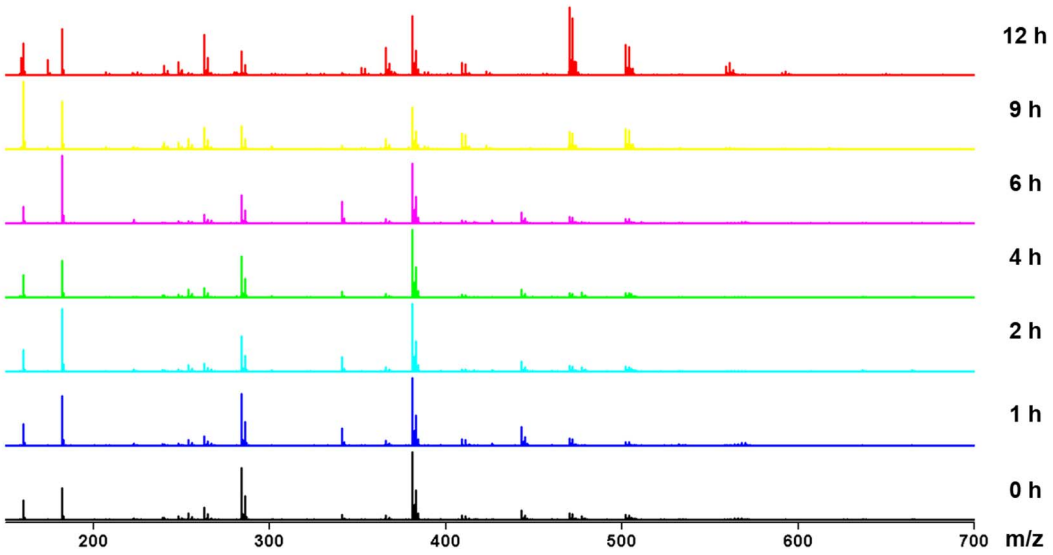

Figure S7. ESI-MS traces the conversion of **Cu1** to **Cu2** in methanol at 60 °C.

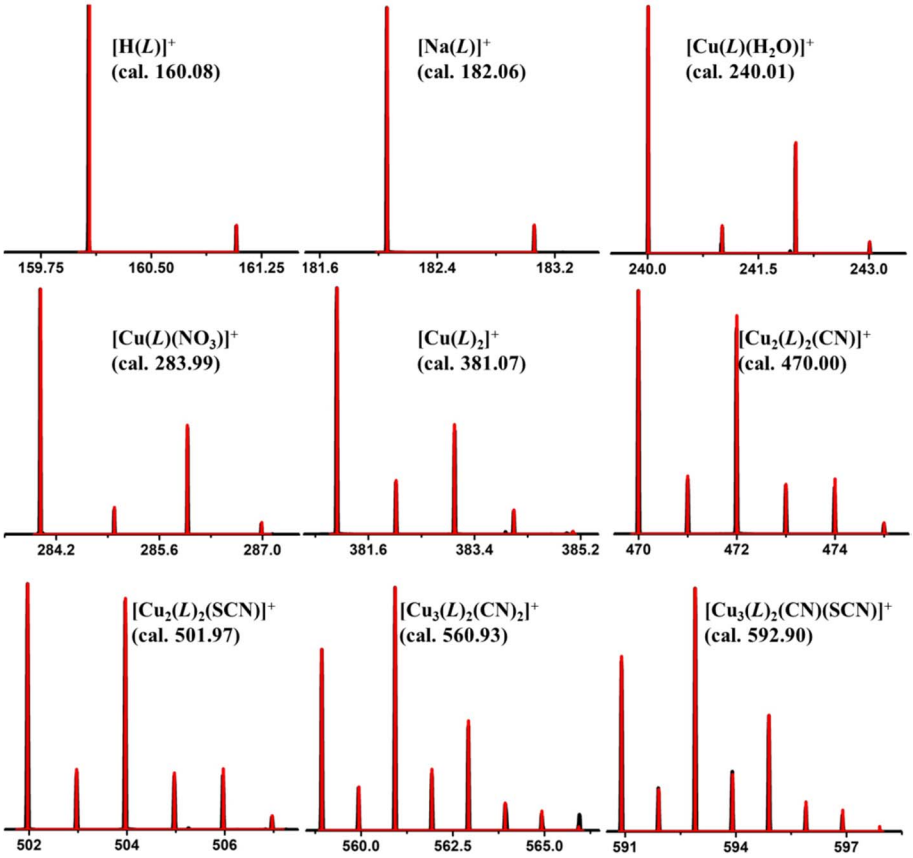

Figure S8. Major species assigned in the ESI-MS of **Cu1** in positive mode.

Table S8. Calculated orbitals energy for ESI-MS fragments using B3LYP functional and SDD (for Fe)/6-311G* (for other elements) with Gaussian 16 software.[1]

Fragments	HOMO/a.u	LUMO/a.u.	Picture	Energy / a.u.
Cu1	Alpha -0.19887 Beta -0.19774	Alpha -0.09270 Beta -0.09205	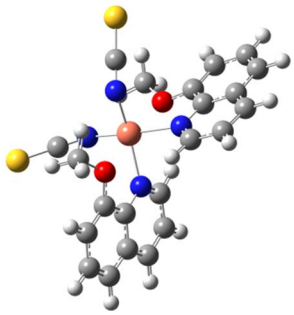	-2212.444236

Cu1-SCN	Alpha -0.46761 Beta -0.46475	Alpha -0.031641 Beta -0.41192	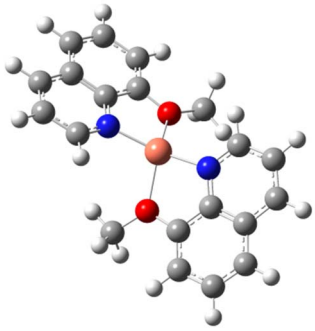	-1229.795349
SCN^-	-0.03989	0.15072	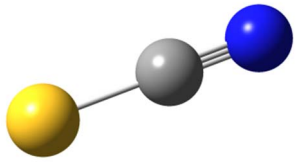	-491.114228
CuL	Alpha -0.55163 Beta -0.55645	Alpha -0.39132 Beta -0.48095	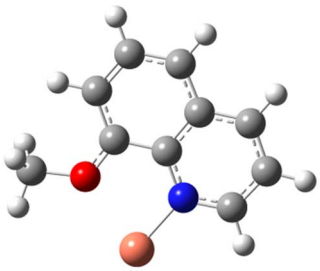	-713.188742
L	-0.21847	-0.05609	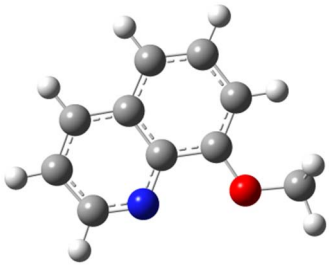	-516.458690
CH_3O^-	0.03973	0.17447	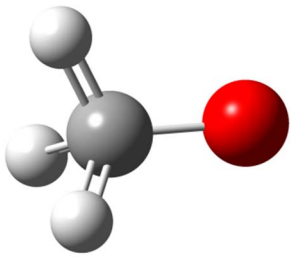	-115.109825

Cu2	Alpha -0.20090 Beta -0.19979	Alpha -0.09425 Beta -0.10574	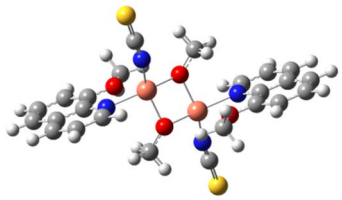	-2640.114553

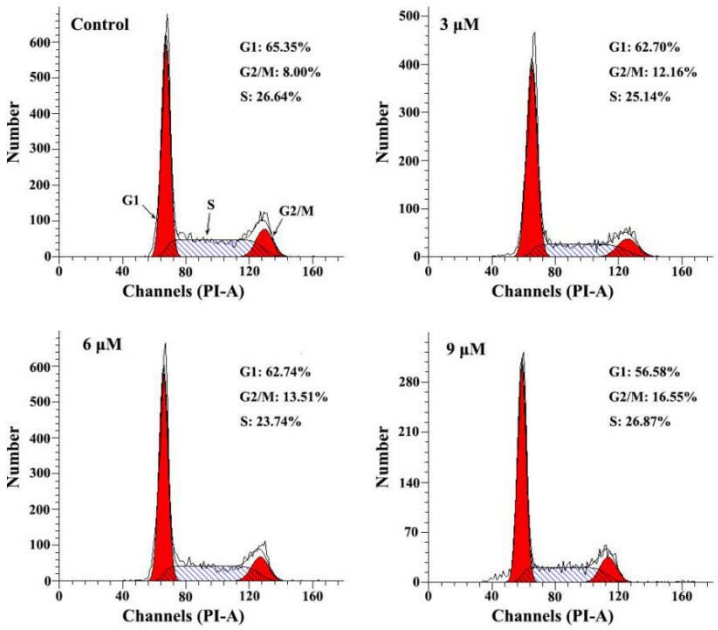

Figure S9. Cell cycle of HeLa tumor cells after treatment with Cu(II) complexes **2** (3 μM, 6 μM, 9 μM) for 24 h compared with untreated cells.

References:

[1] Gaussian 16, Revision A.03, M. J. Frisch, G. W. Trucks, H. B. Schlegel, G. E. Scuseria, M. A. Robb, J. R. Cheeseman, G. Scalmani, V. Barone, G. A. Petersson, H. Nakatsuji, X. Li, M. Caricato, A. V. Marenich, J. Bloino, B. G. Janesko, R. Gomperts, B. Mennucci, H. P. Hratchian, J. V. Ortiz, A. F. Izmaylov, J. L. Sonnenberg, D. Williams-Young, F. Ding, F. Lipparini, F. Egidi, J. Goings, B. Peng, A. Petrone, T. Henderson, D. Ranasinghe, V. G. Zakrzewski, J. Gao, N. Rega, G. Zheng, W. Liang, M. Hada, M. Ehara, K. Toyota, R. Fukuda, J. Hasegawa, M. Ishida, T. Nakajima, Y. Honda, O. Kitao, H. Nakai, T. Vreven, K. Throssell, J. A. Montgomery, Jr., J. E. Peralta, F. Ogliaro, M. J. Bearpark, J. J. Heyd, E. N. Brothers, K. N. Kudin, V. N. Staroverov, T. A. Keith, R. Kobayashi, J. Normand, K. Raghavachari, A. P. Rendell, J. C. Burant, S. S. Iyengar, J. Tomasi, M. Cossi, J. M. Millam, M. Klene, C. Adamo, R. Cammi, J. W. Ochterski, R. L. Martin, K. Morokuma, O. Farkas, J. B. Foresman, and D. J. Fox, Gaussian, Inc., Wallingford CT, 2016.